Upscaling permeability in anisotropic volcanic systems.

Jamie I. Farquharson[a,*], Fabian B. Wadsworth[b,c]

[a]*Géophysique Expérimentale, Institut de Physique de Globe de Strasbourg (UMR 7516 CNRS, Université de Strasbourg/EOST), 5 rue René Descartes, 67084 Strasbourg cedex, France.*
[b]*Department of Earth Sciences, Durham University, Science Labs, Durham DH1 3LE, UK*
[c]*Earth and Environmental Sciences, Ludwig-Maximilians-Universität, Theresienstrasse 41, 80333 München, Germany*

Abstract

Permeability is an increasingly prevalent metric included in volcano modelling; however, it is a property that can exhibit anisotropy in volcanic environments. Permeability of a layered medium can be described by the arithmetic or harmonic means of the permeabilities of the constituent units, depending on the orientation of flow with respect to layering (i.e. flow parallel or perpendicular to layering, respectively). We outline the theory underlying these formulations, and provide experimental permeability data measured on anisotropic volcanic materials in order to demonstrate this point. We highlight that permeability measured parallel to layering or bedding must be higher than that measured perpendicular to layering. Moreover, we emphasise that the choice of averaging method used to upscale permeability data (*i.e.*to calculate the equivalent permeability of a system) has important consequences on the validity of the derived values. We anticipate that these points will help move towards more realistic models of pressure evolution behaviour in volcanoes, and increase the utility of laboratory-derived data for volcano-scale modelling.

Keywords: `Fluid flow, Anisotropy, Soufrière Hills Volcano, Volcán de Colima, Volcano modelling, Upscaling`

1. Introduction

It is well established that permeability—the capacity for fluid flow through a porous or granular medium—is a fundamentally important property influencing pressure generation or release in volcanic systems (e.g. Eichelberger et al., 1986; Melnik et al., 2005). Over the last three decades or so, volcanic rock permeability has become an increasingly prevalent metric with which to discuss mechanisms of volcano outgassing and—in turn—eruption dynamics. Since the work of Eichelberger et al. (1986), numerous studies have examined the permeability of natural and synthetic volcanic materials representing a wide variety of volcanic systems (e.g. Westrich and Eichelberger, 1994; Klug and Cashman, 1996; Mueller et al., 2005; Degruyter et al., 2010; Kolzenburg et al., 2012; Ashwell et al., 2015; Heap et al., 2015; Farquharson et al., 2015, 2016a,b; Wadsworth et al., 2016; Kushnir et al., 2016, 2017a, amongst many others).

Measurements of permeability on centimetric-scale samples—while useful in their own right—do not necessarily reflect the fluid flow characteristics of a volcanic edifice, geothermal reservoir, or any other large system under investigation. Indeed, the ability to "upscale" rock physical properties merits consideration in any case where the scale of measurement is smaller that at which the data are applied. For certain constitutive physical properties, upscaling remains trivial: the average porosity ϕ of a system, for example, is simply the mean value of each of the porosities of the constituent units, which is to say that porosity is an additive, or scalar property. In practice, this means that a theoretical rock mass made up of several smaller units of a given porosity would similarly exhibit that porosity. However many rock physical properties are not scalars, and averaging laws or some other means of upscaling become necessary in order to incorporate measured data into system-scale models (e.g. Tidwell, 1996).

The ability to upscale permeability from the scale of laboratory specimens to that of an outcrop, conduit, or volcanic edifice has been a feature of recent research efforts (e.g. Heap and Kennedy, 2016; Farquharson et al., 2016b, 2017b; Lamur et al., 2017) which have sought to explain the influence of heterogeneities (such as fractures) on the permeability of magma or edifice rock. The inclusion of edifice or magma permeability as a variable parameter has helped move towards more realistic gas evolution models for volcanic systems (Jaupart, 1998; Collombet, 2009; Collinson and Neuberg, 2012; Chevalier et al., 2017). The increased use of laboratory data in numerical models (e.g. Chevalier et al., 2017) is valuable; nevertheless, it is important to note that as this trend continues, the choice of averaging method is ever more critical for accurately transferring data between scales (e.g. Tidwell, 1996).

One of the primary complexities involved in upscaling permeability is the existance of significant anisotropy in the media under investigation. Anisotropy exists in volcanic systems at all scales, and examples of the phenomenon are as myriad as its causes. Magma properties evolve in space and time, resulting in spatially-variable crystal content (e.g. Caricchi et al.,

*Corresponding author
Email address: `farquharson@unistra.fr` (Jamie I. Farquharson)

2007; Vona et al., 2011; Chevrel et al., 2013, 2015), porosity (e.g. Bagdassarov and Dingwell, 1992; Farquharson et al., 2015, 2016b; Wadsworth et al., 2017), and geochemistry (e.g. Giordano et al., 2008). Magma is also buffeted by variations in in-situ stress conditions and strain rate partitioning (e.g. Papale, 1999; Gonnermann and Manga, 2003; Caricchi et al., 2007) within the volcanic conduit—processes that continue during extrusion and emplacement (e.g. Smith et al., 2001; Cashman et al., 2008).

During the ascent, evolution, and eventual emplacement of magma, a host of heterogeneities can form and grow due to mechanisms such as tensile fracturing, partial or complete healing of fractures, cavitation, or inhomogeneous bubble expansion and collapse. Ultimately, this can result in anisotropy on the micro-scale (Farquharson et al., 2016b). Moreover, sequential deposition of volcanic material causes layering or bedding at different scales; indeed, the very definition of a stratovolcano implies anisotropy, in that a typical volcanic edifice is constructed from layers of volcanic material emplaced with a bedding orientation. Figure 1 shows examples of layered volcanic media at different scales.

Permeability of an anisotropic medium is often termed "equivalent" permeabilty, here $\langle k \rangle$, so-called because an anisotropic medium will have a permeability that is *hydraulically equivalent* to a conceptual homogeneous system (Freeze and Cherry, 1979; Renard and De Marsily, 1997). In this contribution, we outline the derivation of this property, and demonstrate—through theory and experiment—that the value of permeability differs with respect to the orientation relative to layering. Finally, we outline the importance of these observations in the context of modelling volcanic systems.

2. Permeability: the fundamentals

Darcy's law (Darcy, 1856) is the constitutive equation governing fluid transport in porous or granular media. Originally derived from experiments performed by Henry Darcy in the 1850s, the theoretical framework of fluid transport—which is based on Newton's second law—has been well established and expanded in the years since.

At a constant elevation, Darcy's law is a proportional relationship between the instantaneous discharge rate Q of a fluid of viscosity μ through a porous medium with cross-sectional area A. Flow is driven over a length L towards the region of lowest potential energy; in the special case of horizontal flow this is defined as the pressure gradient between a point of relatively higher pressure p_b towards a point of relatively lower pressure p_a. Hereafter, we will refer to the absolute value of this pressure gradient $p_b - p_a$ as Δp. Darcy's law is:

$$Q = -\frac{kA}{\mu}\frac{p_b - p_a}{L} \quad \text{or} \quad Q = \frac{kA}{\mu}\frac{\Delta p}{L} \tag{1}$$

where Q is in units of $\mathrm{m^3 s^{-1}}$. We can divide both sides of the equation by the area A, giving a more general notation:

$$q = \frac{k}{\mu}\nabla p \tag{2}$$

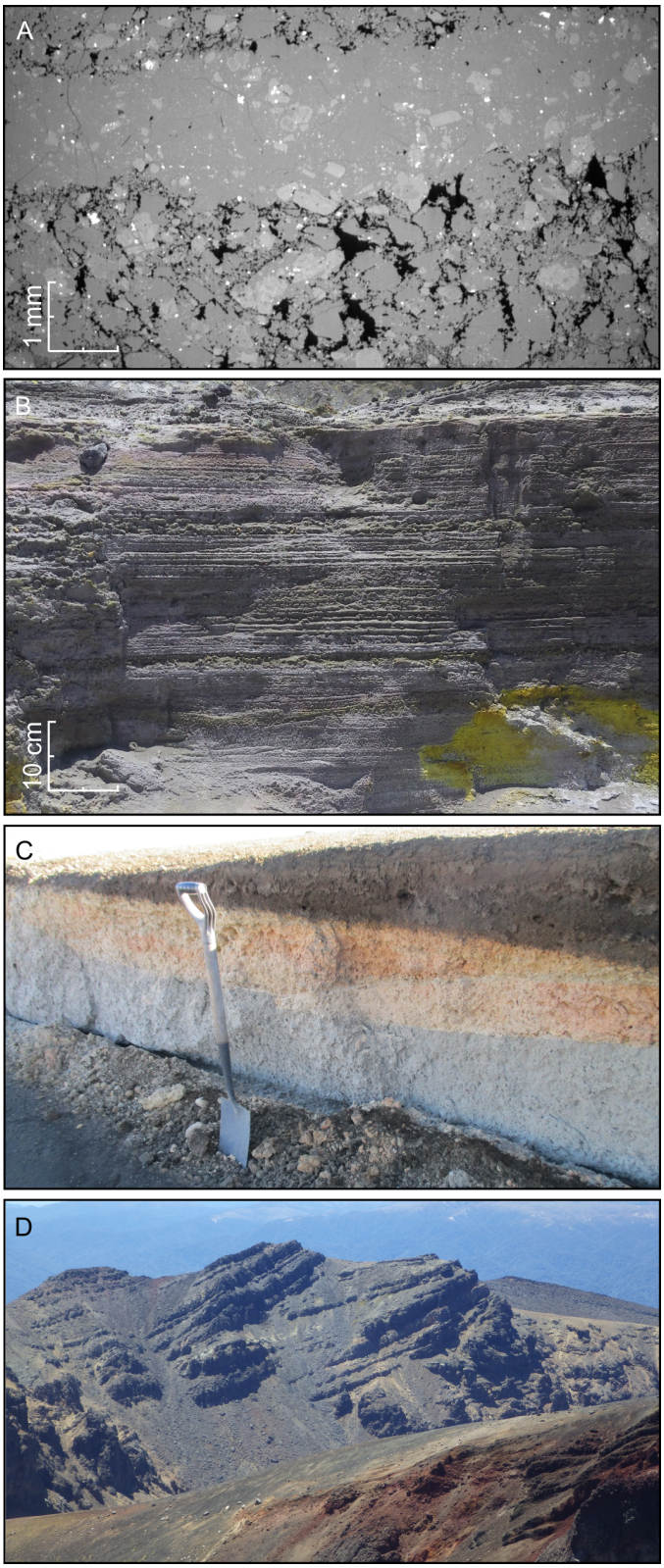

Figure 1: Layering in volcanic environments over different scales. [A] Microstructural anisotropy in banded andesite from Volcán de Colima, Mexico (Farquharson et al., 2016b). Scale is approximate. [B] Finely-bedded tuff layers at Whakaari (White Island), New Zealand. Scale is approximate. [C] Sequentially emplaced layers of the Taupō Ignimbrite, New Zealand. Photo credit: Mike Heap. Spade for scale. [D] Layered lavas, photographed taken looking north from Red Crater towards Te Maari, Tongariro National Park, New Zealand.

where q is the discharge per unit area—also referred to as flux or Darcy velocity—in units of m s^{-1}. (The velocity of fluid flow v through the porosity ϕ of the medium is related to the flux by $v = q/\phi$.) The term ∇p is the pressure gradient vector, equivalent to $\Delta p/L$ and thus has units of Pa m^{-1}.

2.1. Expansion into three dimensions

In three dimensions, the initial Darcy velocity is resolved in three orthagonal directions in a Cartesian coordinate system xyz, giving q_x, q_y, and q_z. Fundamentally. each of these components may exhibit a rate of change, which will depend on the direction in which the change is occurring. The difference between the velocity at any two given points is described by nine components which correspond to each of the directions x, y, and z. Thus:

$$q_x = -\frac{k_{xx}}{\mu}\nabla p_{xx} - \frac{k_{xy}}{\mu}\nabla p_{xy} - \frac{k_{xz}}{\mu}\nabla p_{xz} \tag{3a}$$

$$q_y = -\frac{k_{yx}}{\mu}\nabla p_{yx} - \frac{k_{yy}}{\mu}\nabla p_{yy} - \frac{k_{yz}}{\mu}\nabla p_{yz} \tag{3b}$$

$$q_z = -\frac{k_{zx}}{\mu}\nabla p_{zx} - \frac{k_{zy}}{\mu}\nabla p_{zy} - \frac{k_{zz}}{\mu}\nabla p_{zz} \tag{3c}$$

2.2. Introducing anisotropy

Equations 3a–3c highlight that permeability—in the most general case—similarly comprises nine components. To explain this, we can imagine a vertical section through an anisotropic medium. Permeability at any given point may then expressed by $k = k(\theta)$, where θ is the angle between the horizontal plane and the direction of a measurement of permeability. There exists a mutually orthagonal set of directions where the angle θ corresponds to the maximum and minimum values of k: these are termed the "principal directions of anisotropy" (*e.g.* Renard et al., 2001).

If we array these components in a matrix, permeability becomes a symmetric second-rank tensor, known as the permeability tensor:

$$\langle k \rangle = \begin{bmatrix} k_{xx} & k_{xy} & k_{xz} \\ k_{yx} & k_{yy} & k_{yz} \\ k_{zx} & k_{zy} & k_{zz} \end{bmatrix} \tag{4}$$

where each k_{ij} component corresponds to the coordinates in a Cartesian system. However, it is generally sufficient to assume that the xyz coordinate axes coincide with the principal directions of anisotropy. It follows that we lose the off-diagonal components: $k_{xy} = k_{xz} = k_{yx} = k_{yz} = k_{zx} = k_{zy} = 0$, giving us:

$$\langle k \rangle = \begin{bmatrix} k_{xx} & 0 & 0 \\ 0 & k_{yy} & 0 \\ 0 & 0 & k_{zz} \end{bmatrix}. \tag{5}$$

Moreover, if we consider an anisotropic formation comprised of bedded homogeneous layers—what we can refer to as a transversely isotropic layered medium—then we have $k_{xx} = k_{yy} \neq k_{zz}$. Figure 2 illustrates such a conceptual layered medium.

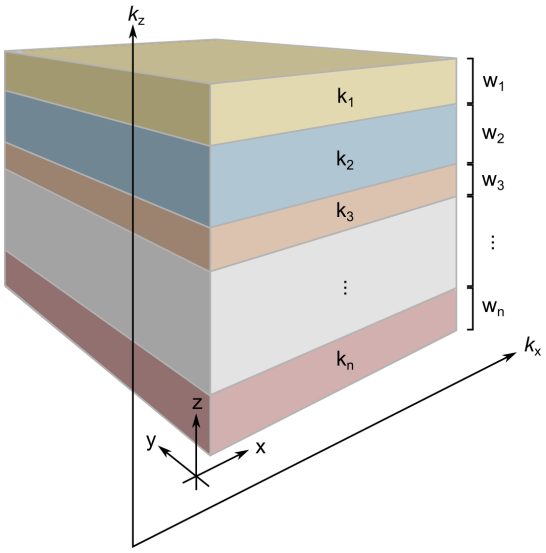

Figure 2: A layered medium. Each of the layers constitutes a homogeneous unit with a width w_i and permeability k_i. Orientation of bedding is such that layers are parallel to x and y, and perpendicular to the z direction. k_x and k_z correspond to the permeability of the (entire) layered medium parallel and perpendicular to bedding, respectively.

For simplicity's sake, we will hereafter discuss permeability in a transversely isotropic system as $\langle k_x \rangle$ and $\langle k_z \rangle$, corresponding to the equivalent permeabilities parallel and perpendicular to layering, respectively.

Let us assume that each of the layers in the anisotropic system of dimensions $L \times L \times L$ (Figure 2) is itself homogeneous in terms of its physical properties. Each layer has a given width $w_1, w_2, w_3, \ldots, w_n$, where n is the total number of layers in the system. The total thickness of the system L may thus be given by the sum of all the layer widths:

$$L = \sum_{i=1}^{n} w_i \tag{6}$$

where w_i refers to the incremental layer width from $i = 1$ to n. Further, each layer has a permeability $k_1, k_2, k_3, \ldots, k_n$.

3. Flow parallel to layering

When flow is parallel to the layering, each of the layers mentioned previously will have certain properties in common. Specifically, the length over which the pressure gradient is occurring —as well the pressure gradient itself—will be identical, as will the fluid viscosity.

The bulk flow rate Q, however, will be partitioned over layers with widths $w_1, w_2, w_3, \ldots, w_n$ such that their areas amount to the total cross-sectional area: $a_1 + a_2 + a_3 + \cdots + a_n = A$. So, if i corresponds to a given layer, it is clear that $Q = \sum_{i=1}^{n} Q_i$ (where Q_i is the flow rate through layer i) and $A = \sum_{i=1}^{n} a_i$. Equivalently we can decompose the area into its constituent width w_i and length l components, giving: $A = \sum_{i=1}^{n} w_i l$. With these

points in mind, we may now re-interrogate Darcy's law (Equation 1) leading us to:

$$Q_1 = \frac{k_1 w_1 l \Delta p}{\mu L}, Q_2 = \frac{k_2 w_2 l \Delta p}{\mu L}, Q_3 = \frac{k_3 w_3 l \Delta p}{\mu L}, \ldots, Q_n = \frac{k_n w_n l \Delta p}{\mu L}. \tag{7}$$

The equivalent permeability $\langle k_x \rangle$ corresponds to the total flow rate (the summation of flow rates through all individual layers), thus:

$$Q \triangleq \sum_{i=1}^{n} Q_i = \frac{k_x A \Delta p}{\mu L} = \left(\frac{k_1 w_1 l \Delta p}{\mu L} + \frac{k_2 w_2 l \Delta p}{\mu L} + \frac{k_3 w_3 l \Delta p}{\mu L} + \cdots + \frac{k_n w_n l \Delta p}{\mu L} \right), \tag{8}$$

which simplifies and rearranges to

$$\langle k_x \rangle = \frac{\sum_{i=1}^{n} w_i k_i}{L}. \tag{9}$$

Equation 9 is the "arithmetic mean" permeability, and is dominated by the layers of highest permeability.

4. Flow perpendicular to layering

If we consider flow perpendicular to layering (i.e. permeability in series), then the volumetric flow rate Q must be equal entering and exiting the system. Indeed, it must be constant at any point in the system. However, the overall pressure differential Δp is partitioned between layers of thickness $w_1, w_2, w_3, \ldots, w_n$, becoming $\Delta p_1, \Delta p_2, \Delta p_3, \ldots, \Delta p_n$. And so:

$$\Delta p_1 = \frac{Q \mu w_1}{k_1 A}, \Delta p_2 = \frac{Q \mu w_2}{k_2 A}, \Delta p_3 = \frac{Q \mu w_3}{k_3 A}, \ldots, \Delta p_n = \frac{Q \mu w_n}{k_n A} \tag{10}$$

In this case, the equivalent permeability $\langle k_z \rangle$ corresponds to the total pressure differential (the summation of pressure drops across all individual layers), thus:

$$\Delta p \triangleq \sum_{i=1}^{n} \Delta p_i = \frac{Q \mu L}{k_z A} = \left(\frac{Q \mu w_1}{k_1 A} + \frac{Q \mu w_2}{k_2 A} + \frac{Q \mu w_3}{k_3 A} + \cdots + \frac{Q \mu w_n}{k_n A} \right) \tag{11}$$

which rearranges and simplifies to

$$\langle k_z \rangle = \frac{L}{\sum_{i=1}^{n} \frac{w_i}{k_i}} \quad \text{or} \quad \langle k_z \rangle = \frac{\sum_{i=1}^{n} w_i}{\sum_{i=1}^{n} \frac{w_i}{k_i}} \tag{12}$$

Equation 12 is the "harmonic mean" permeability, and is dominated by the layers of lowest permeability.

5. Permeability in heterogeneous systems

Equation 9 and 12 correspond to the maximum and minimum equivalent permeabilities within a layered system, so it is to be expected that the equivalent permeability of any heterogeneous system will fall between these end-member values (e.g. Cardwell Jr et al., 1945). For example, a commonly employed averaging method is the geometric mean:

$$\langle k_g \rangle = \exp \left[\frac{\sum_{i=1}^{n} w_i \ln k_i}{\sum_{i=1}^{n} w_i} \right] \tag{13}$$

Computational modelling (Warren and Price, 1961) has been used to show that $\langle k_g \rangle$ can provide a good representation of the equivalent permeability of a random heterogeneous medium. Nevertheless, care should be taken when applying the geometric mean equivalent permeability to highly heterogeneous systems (Jensen, 1991). A notable issue is that $\langle k_g \rangle \to 0$ when any of the constituent layers are close to impermeable, and unphysical values may be derived. Nevertheless, Jensen (1991)—based on theoretical approaches by Bakr et al. (1978); Gutjahr et al. (1978); Dagan (1979, 1981) amongst others—highlights that the geometric mean approach is a suitable means of assessing equivalent permeability if the measured permeabilities $k_1, k_2, k_3, \ldots, k_n$ are log-normally distributed and display low variance. Jensen (1991) also introduces an approach termed the "j^{th} Winsorized mean", which involves censoring extreme values of k_i and replacing them with adjacently ranked data, prior to calculating $\langle k_g \rangle$.

For typical systems $\langle k_x \rangle > \langle k_g \rangle > \langle k_z \rangle$; indeed, for any given set of w_i and k_i, we can assert that $\langle k_x \rangle$ is greater than $\langle k_z \rangle$ (i.e. permeability parallel to layering in a natural system is *always* higher than permeability perpendicular to layering). A simple proof is offered in Appendix A, and we demonstrate this experimentally in the following section. Each of the averaging approaches discussed here are special cases of power-law averaging, a general analytical function. More complex power-law approaches have been employed to estimate hydraulic conductivity in previous studies, typically relating the conductivity of a system to the spatial correlation (or the degree thereof) of individual, variably-permeable units. Such methods include spatial averaging (*e.g.* Deutsch, 1989) and renormalisation averaging (*e.g.* Piggott and Elsworth, 1992), but shall not be discussed further in this study.

In the context of upscaling permeability to applied systems, it is worth noting that these relatively simple averaging approaches may be further expanded in order to account for more complex system geometries. Both arithmetic and harmonic permeabilities may be applied to layered radial flow systems, for example, which could conceivably be of importance in volcanic and geothermal systems. In the first instance, fluid transport parallel to layering in a system of layered disks can be described by Equation 9 without modification (Figure 3A). Fluid transport perpendicular to layering in a system of annular units concentric to a central bore (representing a volcanic conduit or a geothermal well, for example) can be described by a modification of the harmonic average approach. In such a case, permeability must be weighted according to the distances of each concentric unit from the central point (e.g. Cardwell Jr et al.,

1945), therefore:

$$\langle k_r \rangle = \ln\left(\frac{r_a}{r_b}\right) \sum_{i=1}^{n} \left[\ln\left(\frac{r_i}{r_{i-1}}\right) k_i^{-1} \right]^{-1} . \quad (14)$$

r_a and r_b are the central bore radius and the far-field radius, respectively. Values of r_i represent the incremental concentric radii of annular units. This is illustrated in Figure 3B.

There are numerous scenarios wherein a volcanic edifice could be reasonably and usefully conceived as a transversely isotropic layered medium as illustrated in Figure 3A. Stratovolcanoes are constructed from heterogeneous layers of eruptive material—which may possess distinct physical and mechanical properties (Gudmundsson and Brenner, 2004)—and are often modelled as such (*e.g.* Bakker et al., 2016). It has been observed that permeability may differ markedly depending on the subsurface stratigraphy (*e.g.* Watanabe et al., 2008). Indeed, even in a mechanically and compositionally homogeneous volcanic rock mass, permeability may be influenced by lithostatic pressure, effectively creating isobaric strata of differing permeability. This is supported by experiments by Nara et al. (2011), amongst others.

Equally, there are circumstances where the permeability profile of a volcanic edifice may be imagined as an annular concentric structure (*i.e.* Figure 3B). Shear in volcanic conduits is often posited to give rise to conduit-parallel strain localisation (*e.g.* Gonnermann and Manga, 2003; Tuffen and Dingwell, 2005; Plail et al., 2014). In turn, strain localisation in magma can influence permeability (*e.g.* Okumura et al., 2013; Farquharson et al., 2016b). Further, volcano modelling (for example by Hurwitz et al., 2003; Lillis et al., 2015; Schauroth et al., 2016; Bakker et al., 2016; Heap et al., 2017) often assumes a radial thermal gradient from the conduit into the edifice, a parameter which has been shown to influence permeability and permeability evolution (Gaunt et al., 2016; Kushnir et al., 2017b).

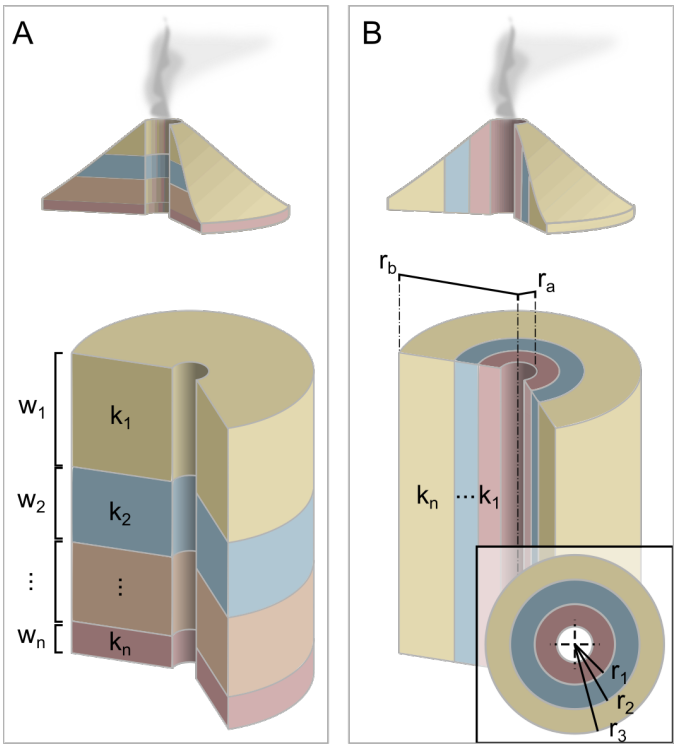

Figure 3: Schematics of simple three-dimensional systems. [A] A system of layered disks, each with width $w_1, w_2, \ldots, w_n$ and corresponding values of permeability. [B] A concentric annular system, where layers are described by their radii (*e.g.* r_1, r_2, r_3: inset) with respect to the radii defining the system (r_a, r_b): those of the inner bore and the far-field radius, respectively. Cartoons highlight how these geometries could be applied to idealised volcanic systems.

6. Anisotropy in natural volcanic samples

6.1. *Soufrière Hills volcano banded pumice*

In the previous section, we stated that permeability parallel to layering must be greater than permeability perpendicular to layering. To demonstrate this, we provide measurements of permeability for a suite of variably-banded pumice samples. The samples were cored from a single block, collected from the Belham river valley on the island of Montserrat during a field campaign in 2012. The block presumably derived from the 11 February 2010 lateral collapse of the Soufrière Hills volcano dome, as described by Stinton et al. (2014). This block was selected because it demonstrates centimetric-scale banding, such that the derived samples exhibit relatively regular layering or lighter- and darker-coloured material (Figure 4). Similarly heterogeneous pumice was noted following the 1997 explosive eruption of Soufrière Hills volcano by Burgisser et al. (2010) and others, as well as in other explosive volcanic environments around the globe (Venezky and Rutherford, 1997; Hall et al., 1999; Kennedy et al., 2005; De Maisonneuve et al., 2009; Farquharson et al., 2016b). Whilst we presume the bands originated in the block of this study due to inhomogeneous bubble expansion or compaction whilst still deforming viscously prior to emplacement (e.g. Farquharson et al., 2016b)—as a result of the complex decompression mechanisms associated with the 2011 dome collapse—we note that banding in pumice has been variously attributed to magma mingling, variations in magma differentiation, or variability in dissolved water content as well as inhomogenous bubble extension processes.

Samples were prepared such that they had diameters of 20 mm and were nominally 40 mm in length (samples are shown in Figure 4). Connected gas porosity ϕ was determined using helium pycnometry, and permeability was measured using a steady-state benchtop permeameter (see Heap and Kennedy, 2016; Farquharson et al., 2016b, for a schematic). Full details are provided in Appendix B. Table 1 displays the porosity and permeability data of the 20 samples. Permeability is plotted against connected gas porosity for the Soufrière Hills volcano samples in Figure 5. Clearly, the samples exhibiting layering parallel and perpendicular to the sample axis (and thus the direction of measurement: $\langle k_x \rangle$ and $\langle k_z \rangle$, respectively) comprise two distinct families on the graph, with the former tending to exhibit relatively higher permeability. The degree of scatter in these data is presumably a function of the naturally variable volume and geometry of the layers within the sample suite (as

Table 1: Connected porosity ϕ and permeability k data for 20 Soufrière Hills volcano banded pumice samples. Permeability was measured parallel $\parallel$ or perpendicular $\perp$ to banding.

Sample	ϕ	k [m^2]	
SHV-X-1	0.32	1.10×10^{-12}	$\parallel$
SHV-X-2	0.33	2.41×10^{-13}	$\parallel$
SHV-X-3	0.33	1.06×10^{-12}	$\parallel$
SHV-X-4	0.32	9.15×10^{-13}	$\parallel$
SHV-X-5	0.32	4.07×10^{-13}	$\parallel$
SHV-X-6	0.32	4.43×10^{-13}	$\parallel$
SHV-X-7	0.33	7.18×10^{-13}	$\parallel$
SHV-X-8	0.34	1.73×10^{-12}	$\parallel$
SHV-X-9	0.34	1.69×10^{-12}	$\parallel$
SHV-X-10	0.34	1.31×10^{-12}	$\parallel$
SHV-X-11	0.33	4.30×10^{-13}	$\parallel$
SHV-Z-1	0.30	1.07×10^{-13}	$\perp$
SHV-Z-2	0.32	1.74×10^{-13}	$\perp$
SHV-Z-3	0.34	3.63×10^{-13}	$\perp$
SHV-Z-4	0.30	2.01×10^{-13}	$\perp$
SHV-Z-5	0.31	1.64×10^{-13}	$\perp$
SHV-Z-6	0.30	2.35×10^{-13}	$\perp$
SHV-Z-7	0.31	1.41×10^{-13}	$\perp$
SHV-Z-8	0.30	3.02×10^{-13}	$\perp$
SHV-Z-9	0.31	2.16×10^{-13}	$\perp$

evident in Figure 4). Nevertheless, these data highlight that permeability may vary significantly when anisotropy is investigated. For example, samples SHV-X-8 and SHV-Z-3, which have the same connected porosity (0.34) but were obtained and measured in orthagonal directions, differ by a factor of 5 in terms of their permeability (Table 1, Figure 5).

6.2. *Volcán de Colima flow-banded lava*

Three permeability averaging methods have been advanced in the preceding sections: arithmetic, harmonic, and geometric means (Equation 9, 12, and 13, respectively), with the assertion that they should best describe certain layered systems. To verify this, we use permeability data from cores of a flow-banded lava block collected from "El Volcancito", a parasitic dome on the north-eastern flank of Volcán de Colima, Mexico (see Farquharson et al., 2016b, for more information). The initial block was a dense lava exhibiting meso-scale anisotropy whereby half of the block appeared dark grey in colour and the other half was visibly lighter in colour (see Figure 6: inset). Farquharson et al. (2016b) prepared samples cored parallel and perpendicular to the interface between the two textures, including samples encompassing the interface in either orientation (Figure 6). Sample preparation and measurement were performed as described in the preceding section and Appendix B; however, the Forchheimer correction was not necessary for these data.

Due to the relatively simple geometry of the sample-scale heterogeneities, this sample suite can be used to assess the validity of the three permeability averaging approaches. For the layered samples in either orientation, it should be possible to calculate their equivalent permeability $\langle k \rangle$ given knowledge of the width (or area, as appropriate) of either layer and their respective permeabilities.

Figure 6 shows the six samples discussed in this section. For the samples cored in the z direction (Figure 6A), the permeabilities of the dark- and light-grey parts of the block are referred to as k_1 and k_2, respectively. The permeability of the layered sample shall be given as $\langle k_\perp \rangle$: a function of the ratio of thickness of either component (w_1 and w_2), which were measured with digital callipers (Table 2). Similarly, for the samples cored in the x direction (Figure 6B), the permeabilities of the dark- and light-grey parts of the block are referred to as k_3 and k_4, respectively, and the equivalent permeability of the sample shall be referred to as $k_\parallel$. Due to the cylindrical geometry of the samples, we cannot simply use the w_3 and w_4 dimensions (Figure 6B). Instead, we use the average cross-sectional area of each component (dark grey vs. light grey), which we present in Table 2 as a_3 and a_4. These values were determined by binarising digital photographs of either face of the sample, then normalising the output pixel area to the true total area of the cylindrical cross-section. For calculations, each w_i parameter in Equation 9, 12, and 13 was substituted for a_i, thereby translating the averages into two dimensions rather than one (*e.g.* Heap and Kennedy, 2016). All of the permeability data shown in Table 2 are taken from Farquharson et al. (2016b).

First, we shall look at the layered sample cored perpendicular to layering, $k_\perp$ (see Figure 6A). Accounting for potential innacuracies in band geometry, the values determined using Equation 9, 12, and 13 are:

$\langle k_x \rangle = 6.82 \times 10^{-15} \pm 1.23 \times 10^{-15}$ m^2,
$\langle k_z \rangle = 5.54 \times 10^{-16} \pm 8.11 \times 10^{-17}$ m^2, and
$\langle k_g \rangle = 1.90 \times 10^{-15} \pm 5.64 \times 10^{-16}$ m^2, respectively. The true (measured) value is:
$k_\perp = 2.48 \times 10^{-16}$ m^2.

For the sample cored parallel to layering, $k_\parallel$ (see Figure 6B), we obtain the following values for each of the averaging approaches (Equation 9, 12, and 13):

$\langle k_x \rangle = 3.65 \times 10^{-15} \pm 7.58 \times 10^{-17}$ m^2,
$\langle k_z \rangle = 8.77 \times 10^{-16} \pm 8.07 \times 10^{-17}$ m^2, and
$\langle k_g \rangle = 1.48 \times 10^{-15} \pm 2.89 \times 10^{-16}$ m^2, respectively. The true (measured) value is:
$k_\parallel = 3.03 \times 10^{-15}$ m^2.

These data are shown graphically in Figure 7. In both cases, $\langle k_x \rangle > \langle k_g \rangle > \langle k_z \rangle$, and there is no overlap between calculated values. For the perpendicular sample, $k_\perp$ is lower than any of the calculated values; however, the harmonic mean $\langle k_z \rangle$ provides the closest estimate, as predicted. The discrepancy between the measured and calculated value here is perhaps due to variations in band thickness *inside* the sample, thus not reflected in the measured values of w_1 and w_2. We also highlight that the data are used assuming no errors in permeability measurement. For the parallel sample, $k_\parallel$ is exactly within the range calculated from the arithmetic mean, which—again—supports

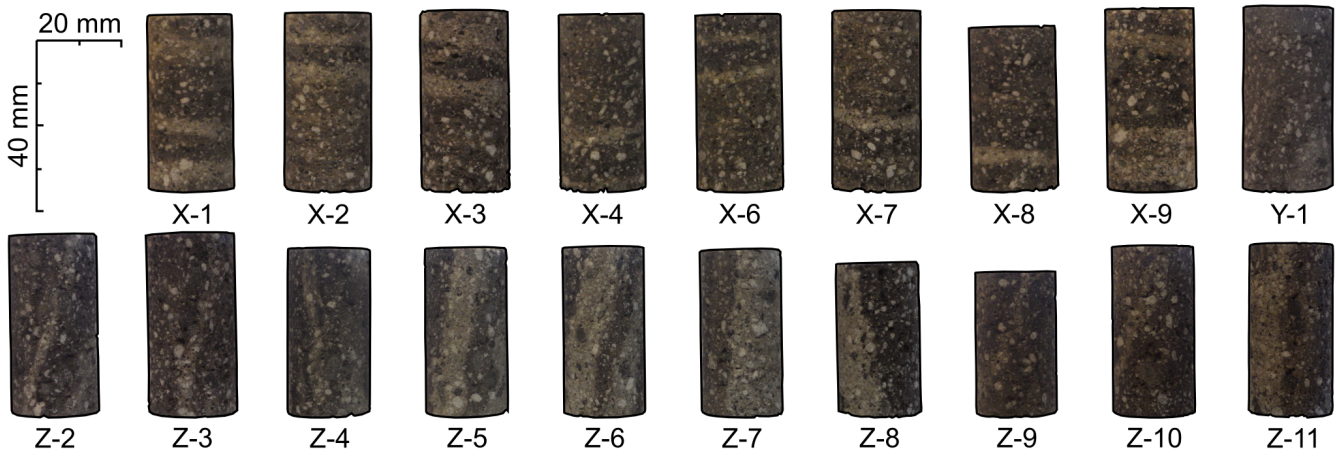

Figure 4: Soufrière Hills volcano pumice samples. Samples X-1—X-9 exhibit banding perpendicular to the sample axis. Samples Z-1—Z-11 exhibit banding parallel to the sample axis. Sample X-5 is not shown, as it was lost in the post.

our previous assertion. Notably, using an inappropriate averaging method could yield results almost an order of magnitude away from the true value. Moreover, it is clear that should the geometric averaging method be employed in this instance, one might incorrectly assume that $k_\perp > k_\parallel$, which is evidently not the case. Nevertheless, if the precise geometry and orientation of an anisotropic medium is unknown, the geometric average may provide a reasonable compromise between the direction-specific arithmetic and harmonic averages (provided the caveats mentioned previously are adhered to: normal distribution and low variance of permeability).

We have used to end-members as a case study (banding is layered at $\pi/2$ and π rad relative to the direction of fluid flow). If the orientation of anisotropy occurs at angles between $\pi/2$ and π rad (*i.e.*neither perpendicular nor parallel to the direction of fluid flow), the fluid flow properties become more complex. In such a case, the principal directions of anisotropy no longer coincide with the Cartesian xyz coordinate system, and permeability is thus less readily analytically approximated. As touched upon in previous sections, the relative importance of the highest and lowest permeability layers is a function of the angle of anisotropy. Thus, steep-angle layering (orientation close to π) will exhibit $\langle k \rangle$ close to $\langle k_\parallel \rangle$ and shallow-angle layering (orientation close to $\pi/2$) will $\langle k \rangle$ close to $\langle k_\perp \rangle$. This concept is approximated by the dashed line on Figure 7.

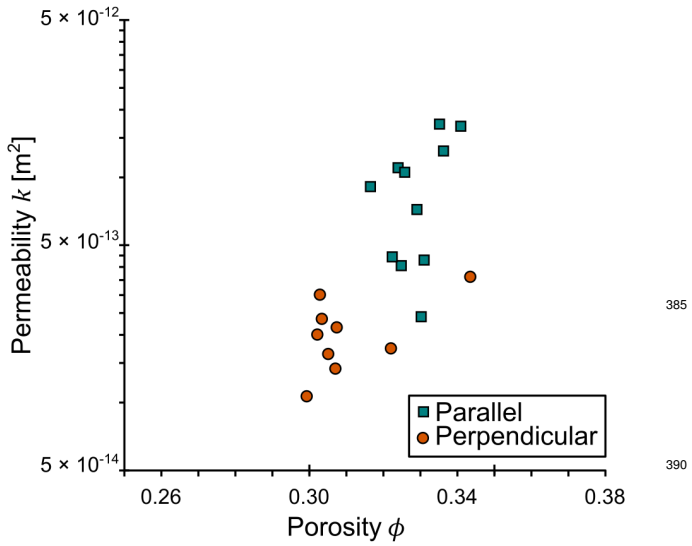

Figure 5: Connected porosity and permeability data for the Soufrière Hills volcano banded pumice samples.

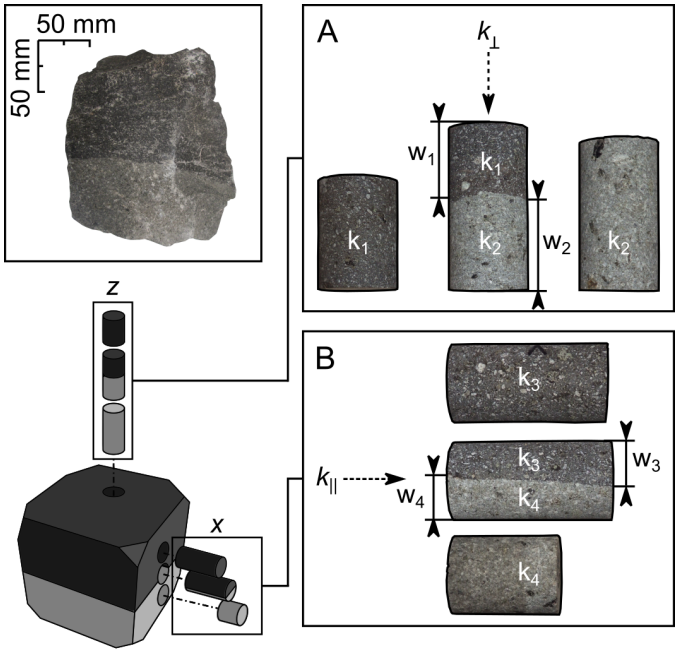

Figure 6: Samples of Col-V-5 in z and x directions. [A] Samples cored in the z direction. [B] Samples cored in the x direction. Block shown in inset. Permeability measured in the direction of the dashed arrow in either case. See Farquharson et al. (2016b) for more information.

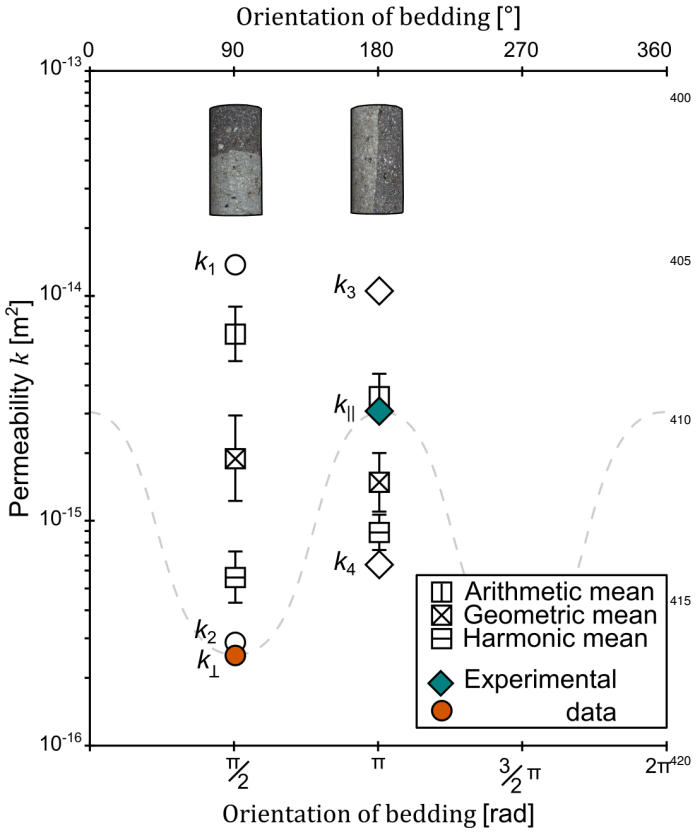

Figure 7: Measured and calculated permeability for banded lava, plotted versus the orientation of banding with respect to the sample axis. $k_\perp$ and $k_\parallel$ are given by the filled symbols, and the empty symbols indicate the values of k_i (Table 2). The range of values of the arithmetic, harmonic, and geometric means (based on the data in Table 2) are shown by the error bars. Refer to text for discussion.

Table 2: Values used for calculating arithmetic, geometric, and harmonic mean permeabilities. $k_1 \ldots k_4$ are permeabilities as indicated in Figure 6. Along with the values of $k_\perp$ and $k_\parallel$, these have been taken from Farquharson et al. (2016b). w_1 and w_2 represent band thickness as shown in Figure 6. a_3 and a_4 are cross-sectional areas of the bands represented by w_3 and w_4, respectively, in Figure 6. Refer to text for discussion.

Parameter	Value	Units
k_1	1.37×10^{-14}	m^2
k_2	2.90×10^{-16}	m^2
k_3	1.05×10^{-14}	m^2
k_4	6.24×10^{-16}	m^2
w_1	19.93 ± 3.75	mm
w_2	20.98 ± 3.75	mm
a_3	96.30 ± 24.13	mm^2
a_4	218.01 ± 24.13	mm^2
$k_\perp$	2.48×10^{-16}	m^2
$k_\parallel$	3.03×10^{-15}	m^2

7. Concluding remarks

Using laboratory measurements on two suites of anisotropic volcanic rocks, we have demonstrated two fundamental points to account for when considering permeability in anisotropic volcanic systems.

1. First, whenever a layered medium contains layers with different permeabilities, the permeability parallel to layering will *always* be higher than that measured perpendicular.
2. Secondly, the choice of averaging method used to upscale permeability data is of great importance. Our data highlight that employing an inappropriate upscaling approach can result in data that are erroneous by almost an order of magnitude (for the samples tested in this study). Significantly, using an inappropriate averaging method can result in values that are contrary to point 1.

We have highlighted scenarios where a volcano could be modelled as a vertically or horizontally layered medium (in two dimensions) or layered disks or an annular concentric medium (in three dimensions), depending on the variables under consideration. As shown both by theory and our data, the averaging method used to estimate equivalent permeability—an imperative step for transferring permeability from the laboratory- to model-scale—can exert a significant influence on the ultimate values derived. We urge that future models that include edifice and/or conduit permeability as a variable—whether to describe the evolution of gas pressure or temperature diffusion in volcanic systems—account for the potential for significant permeability anisotropy in these systems. Moreover, we recommend that the simple formulations described herein be used to transfer the wealth of laboratory data collected on volcanic media to scales that are relevant for edifice-scale modelling.

Acknowledgements

We acknowledge Jackie Kendrick, Bettina Scheu, Yan Lavallée, Jérémie Vasseur, and Linda Petrakova for field assistance on the island of Montserrat. Mike Heap and Nick Varley are thanked for assistance in the field in Mexico, and Mike is additionally thanked for his assistance during sample preparation and characterisation. This paper benefitted from conversations with Luke Griffiths and Alex Kushnir.

Appendix A. Arithmetic mean is always greater than the harmonic mean in an anisotropic medium: proof

This appendix outlines a proof of the assertion that the arithmetic mean of a set of values (such as permeability measurements) is always greater than the harmonic mean of the same set. For a more comprehensive proof, please refer to Binmore (1982).

We may define the arithmetic mean $\langle x \rangle$ of a set of measurements or observations $x_1, x_2, x_3, \ldots, x_n$ as

$$\langle x \rangle = \frac{1}{n}\left(\sum_{i=1}^{n} x_i\right) \tag{A.1}$$

as long as the observations are positive integers (i.e. $x_1, x_2, x_3, \ldots, x_n \in \mathbb{R}_{>0}$). The harmonic mean $\langle z \rangle$ may be cast as:

$$\frac{1}{\langle z \rangle} = \frac{1}{n}\left(\sum_{i=1}^{n} \frac{1}{x_i}\right) \tag{A.2}$$

for all values of i that are positive real numbers ($\forall_i \in [1 \ldots n] : x_i > 0$). Fundamentally, these expressions (Equation A.1 and A.2) are the same as Equation 9 and 12. The corollary of the positive real numbers caveat is that both $\langle x \rangle$ and $\langle z \rangle$ may be expressed as a squared quantity:

$$\forall_i \in [1 \ldots n] : x_i = y_i^2. \tag{A.3}$$

This gives us

$$\langle x \rangle = \frac{1}{n}\left(\sum_{i=1}^{n} y_i^2\right) \text{ and } \frac{1}{\langle z \rangle} = \frac{1}{n}\left(\sum_{i=1}^{n} \frac{1}{y_i^2}\right) \tag{A.4}$$

If we multiply these two expressions together:

$$\langle x \rangle \times \frac{1}{\langle z \rangle} = \frac{\langle x \rangle}{\langle z \rangle} = \frac{1}{n^2}\left(\sum_{i=1}^{n} y_i \sum_{i=1}^{n} \frac{1}{y_i}\right)^2 \tag{A.5}$$

Cauchy's inequality (in vector form: $\|\mathbf{a}\|\,\|\mathbf{b}\| \geq \|\mathbf{a} \cdot \mathbf{b}\|$) tells us that

$$\frac{1}{n^2}\left(\sum_{i=1}^{n} y_i \sum_{i=1}^{n} \frac{1}{y_i}\right)^2 \geq \frac{1}{n^2}\left(\sum_{i=1}^{n} \frac{y_i}{y_i}\right)^2 \tag{A.6}$$

The right-hand-side reduces to unity, giving

$$\frac{\langle x \rangle}{\langle z \rangle} \geq 1 \tag{A.7}$$

and finally

$$\langle x \rangle \geq \langle z \rangle. \tag{A.8}$$

As the equality of $\langle x \rangle = \langle z \rangle$ (in the context of a permeable system $\langle k_x \rangle = \langle k_z \rangle$) requires a homogenous system, we can thus state that for any anisotropic system, $\langle k_x \rangle > \langle k_z \rangle$.

Appendix B. Gas permeability measurements with turbulence

When using a compressible gas as the permeant fluid, it becomes convenient to present permeability measured under near-atmospheric conditions in the form (Klinkenberg et al., 1941; McPhee and Arthur, 1991)

$$k_{gas} = \frac{Q\mu L \cdot p_{atm}}{A \cdot \Delta p \bar{p}}. \tag{B.1}$$

Functionally the same as Equation 1, the above form describes the driving force for flow in terms of a driving pressure $\Delta p \bar{p}$ and a downstream pressure (which in our case is atmospheric pressure p_{atm}) at which Q is measured. The mean pressure $\bar{p}$ is a function of the upstream and downstream pressures p_b and p_a (as described in Farquharson et al., 2017a). We measured gas permeability using a modified steady-state benchtop permeameter as described in (Heap and Kennedy, 2016; Farquharson et al., 2016b). Using nitrogen, a radial confining pressure of 1 MPa was applied to each sample; gas flow was induced through the sample after a suitable equilibration time. For different imposed pressure differentials Δp, the volumetric flowrate Q was measured and recorded with a purpose-built data acquisition system. With knowledge of the contants in Equation B.1 (*i.e.*sample dimensions, atmospheric pressure, gas viscosity), k_{gas} could then be calculated, assuming laminar flow. However, in these high-porosity pumice samples, inertial forces were high (flow was turbulent). As a result, the "true" permeability is lower than the apparent (measured) permeability, as turbulence induces drag. As such, an auxilliary correction was required. The so-called Forchheimer correction, after Forchheimer (1901) introduces an inertial term ι, such that

$$\frac{1}{k_{\mathrm{Fo}}} = \frac{1}{k_{gas}} - \iota Q \tag{B.2}$$

where k_{Fo} is the Forchheimer-corrected permeability value, and k_{gas} is the as-measured value (using gas). This correction is described more fully in Farquharson et al. (2017a).

References

Ashwell, P., Kendrick, J., Lavallée, Y., Kennedy, B., Hess, K.U., Aulock, F., Wadsworth, F., Vasseur, J., Dingwell, D., 2015. Permeability of compacting porous lavas. Journal of Geophysical Research: Solid Earth 120, 1605–1622.

Bagdassarov, N.S., Dingwell, D.B., 1992. A rheological investigation of vesicular rhyolite. Journal of volcanology and geothermal research 50, 307–322.

Bakker, R.R., Frehner, M., Lupi, M., 2016. How temperature-dependent elasticity alters host rock/magmatic reservoir models: A case study on the effects of ice-cap unloading on shallow volcanic systems. Earth and Planetary Science Letters 456, 16–25.

Bakr, A.A., Gelhar, L.W., Gutjahr, A.L., MacMillan, J.R., 1978. Stochastic analysis of spatial variability in subsurface flows: 1. comparison of one-and three-dimensional flows. Water Resources Research 14, 263–271.

Binmore, K.G., 1982. Mathematical Analysis: a straightforward approach. Cambridge University Press.

Burgisser, A., Poussineau, S., Arbaret, L., Druitt, T.H., Giachetti, T., Bourdier, J.L., 2010. Pre-explosive conduit conditions of the 1997 vulcanian explosions at soufrière hills volcano, montserrat: I. pressure and vesicularity distributions. Journal of Volcanology and Geothermal Research 194, 27–41.

Cardwell Jr, W., Parsons, R., et al., 1945. Average permeabilities of heterogeneous oil sands. Transactions of the AIME 160, 34–42.

Caricchi, L., Burlini, L., Ulmer, P., Gerya, T., Vassalli, M., Papale, P., 2007. Non-newtonian rheology of crystal-bearing magmas and implications for magma ascent dynamics. Earth and Planetary Science Letters 264, 402–419.

Cashman, K.V., Thornber, C.R., Pallister, J.S., 2008. From dome to dust: Shallow crystallization and fragmentation of conduit magma during the 2004-2006 dome extrusion of mount st. helens, washington. US Geological Survey professional paper , 387–413.

Chevalier, L., Collombet, M., Pinel, V., 2017. Temporal evolution of magma flow and degassing conditions during dome growth, insights from 2d numerical modeling. Journal of Volcanology and Geothermal Research 333, 116–133.

Chevrel, M., Platz, T., Hauber, E., Baratoux, D., Lavallée, Y., Dingwell, D., 2013. Lava flow rheology: a comparison of morphological and petrological methods. Earth and Planetary Science Letters 384, 109–120.

Chevrel, M.O., Cimarelli, C., deBiasi, L., Hanson, J.B., Lavallée, Y., Arzilli, F., Dingwell, D.B., 2015. Viscosity measurements of crystallizing andesite from tungurahua volcano (ecuador). Geochemistry, Geophysics, Geosystems 16, 870–889.

Collinson, A., Neuberg, J., 2012. Gas storage, transport and pressure changes in an evolving permeable volcanic edifice. Journal of Volcanology and Geothermal Research 243, 1–13.

Collombet, M., 2009. Two-dimensional gas loss for silicic magma flows: toward more realistic numerical models. Geophysical Journal International 177, 309–318.

Dagan, G., 1979. Models of groundwater flow in statistically homogeneous porous formations. Water Resources Research 15, 47–63.

Dagan, G., 1981. Analysis of flow through heterogeneous random aquifers by the method of embedding matrix: 1. steady flow. Water Resources Research 17, 107–121.

Darcy, H., 1856. Les fontaines publiques de la ville de Dijon: Exposition et application des principes à suivre et des formules à employer dans les questions de distribution d'eau. [Exhibition and implementation of the principles to follow and the formulae to employ in the issue of water distribution.] (In French). Victor Dalmont, France.

De Maisonneuve, C.B., Bachmann, O., Burgisser, A., 2009. Characterization of juvenile pyroclasts from the kos plateau tuff (aegean arc): insights into the eruptive dynamics of a large rhyolitic eruption. Bulletin of volcanology 71, 643.

Degruyter, W., Bachmann, O., Burgisser, A., 2010. Controls on magma permeability in the volcanic conduit during the climactic phase of the kos plateau tuff eruption (aegean arc). Bulletin of Volcanology 72, 63.

Deutsch, C., 1989. Declus: a fortran 77 program for determining optimum spatial declustering weights. Computers & Geosciences 15, 325–332.

Eichelberger, J., Carrigan, C., Westrich, H., Price, R., 1986. Non-explosive silicic volcanism. Nature 323, 598–602.

Farquharson, J.I., Baud, P., Heap, M.J., 2017a. Inelastic compaction and permeability evolution in volcanic rock. Solid Earth 8, 561.

Farquharson, J.I., Heap, M.J., Baud, P., 2016a. Strain-induced permeability increase in volcanic rock. Geophysical Research Letters 43.

Farquharson, J.I., Heap, M.J., Lavallée, Y., Varley, N.R., Baud, P., 2016b. Evidence for the development of permeability anisotropy in lava domes and volcanic conduits. Journal of Volcanology and Geothermal Research 323, 163–185.

Farquharson, J.I., Heap, M.J., Varley, N.R., Baud, P., Reuschlé, T., 2015. Permeability and porosity relationships of edifice-forming andesites: a combined field and laboratory study. Journal of Volcanology and Geothermal Research 297, 52–68.

Farquharson, J.I., Wadsworth, F.B., Heap, M.J., Baud, P., 2017b. Time-dependent permeability evolution in compacting volcanic fracture systems and implications for gas overpressure. Journal of Volcanology and Geothermal Research 339, 81–97.

Forchheimer, P., 1901. Wasserbewegung durch boden [water movement through soil.] (in german). Zeitz. Ver. Duetch Ing. 45, 1782–1788.

Freeze, R.A., Cherry, J.A., 1979. Groundwater, 604 pp.

Gaunt, H.E., Sammonds, P.R., Meredith, P.G., Chadderton, A., 2016. Effect of temperature on the permeability of lava dome rocks from the 2004–2008 eruption of mount st. helens. Bulletin of Volcanology 78, 30.

Giordano, D., Russell, J.K., Dingwell, D.B., 2008. Viscosity of magmatic liquids: a model. Earth and Planetary Science Letters 271, 123–134.

Gonnermann, H., Manga, M., 2003. Explosive volcanism may not be an inevitable consequence of magma fragmentation. Nature 426, 432–435.

Gudmundsson, A., Brenner, S.L., 2004. How mechanical layering affects local stresses, unrests, and eruptions of volcanoes. Geophysical Research Letters 31.

Gutjahr, A.L., Gelhar, L.W., Bakr, A.A., MacMillan, J.R., 1978. Stochastic analysis of spatial variability in subsurface flows: 2. evaluation and application. Water Resources Research 14, 953–959.

Hall, M.L., Robin, C., Beate, B., Mothes, P., Monzier, M., 1999. Tungurahua volcano, ecuador: structure, eruptive history and hazards. Journal of Volcanology and Geothermal Research 91, 1–21.

Heap, M., Farquharson, J.I., Wadsworth, F., Kolzenburg, S., Russell, J., 2015. Timescales for permeability reduction and strength recovery in densifying magma. Earth and Planetary Science Letters 429, 223–233.

Heap, M.J., Kennedy, B.M., 2016. Exploring the scale-dependent permeability of fractured andesite. Earth and Planetary Science Letters 447, 139–150.

Heap, M.J., Violay, M., Wadsworth, F.B., Vasseur, J., 2017. From rock to magma and back again: The evolution of temperature and deformation mechanism in conduit margin zones. Earth and Planetary Science Letters 463, 92–100.

Hurwitz, S., Kipp, K.L., Ingebritsen, S.E., Reid, M.E., 2003. Groundwater flow, heat transport, and water table position within volcanic edifices: Implications for volcanic processes in the cascade range. Journal of Geophysical Research: Solid Earth 108.

Jaupart, C., 1998. Gas loss from magmas through conduit walls during eruption. Geological Society, London, Special Publications 145, 73–90.

Jensen, J.L., 1991. Use of the geometric average for effective permeability estimation. Mathematical geology 23, 833–840.

Kennedy, B., Spieler, O., Scheu, B., Kueppers, U., Taddeucci, J., Dingwell, D.B., 2005. Conduit implosion during vulcanian eruptions. Geology 33, 581–584.

Klinkenberg, L., et al., 1941. The permeability of porous media to liquids and gases, in: Drilling and production practice, American Petroleum Institute.

Klug, C., Cashman, K.V., 1996. Permeability development in vesiculating magmas: implications for fragmentation. Bulletin of Volcanology 58, 87–100.

Kolzenburg, S., Heap, M., Lavallée, Y., Russell, J., Meredith, P., Dingwell, D.B., 2012. Strength and permeability recovery of tuffisite-bearing andesite. Solid Earth 3, 191.

Kushnir, A.R., Martel, C., Bourdier, J.L., Heap, M.J., Reuschlé, T., Erdmann, S., Komorowski, J.C., Cholik, N., 2016. Probing permeability and microstructure: Unravelling the role of a low-permeability dome on the explosivity of merapi (indonesia). Journal of Volcanology and Geothermal Research 316, 56–71.

Kushnir, A.R., Martel, C., Champallier, R., Arbaret, L., 2017a. In situ confirmation of permeability development in shearing bubble-bearing melts and implications for volcanic outgassing. Earth and Planetary Science Letters 458, 315–326.

Kushnir, A.R.L., Martel, C., Champallier, R., Wadsworth, F., 2017b. Permeability evolution in variably glassy basaltic andesites measured under magmatic conditions. Geophysical Research Letters 44.

Lamur, A., Kendrick, J., Eggertsson, G., Wall, R., Ashworth, J., Lavallée, Y., 2017. The permeability of fractured rocks in pressurised volcanic and geothermal systems. Scientific Reports 7, 6173.

Lillis, R.J., Dufek, J., Kiefer, W.S., Black, B.A., Manga, M., Richardson, J.A., Bleacher, J.E., 2015. The syrtis major volcano, mars: A multidisciplinary approach to interpreting its magmatic evolution and structural development. Journal of Geophysical Research: Planets 120, 1476–1496.

McPhee, C.A., Arthur, K.G., 1991. Klinkenberg permeability measurements: problems and practical solutions, in: Advances in Core Evaluation IL Reservoir Appraisal, Proceedings of the 2nd Society of Core Analysts European Core Analysis Symposium, Gordon & Breach Science Publishers, Philadelphia, pp. 371–391.

Melnik, O., Barmin, A., Sparks, R., 2005. Dynamics of magma flow inside volcanic conduits with bubble overpressure buildup and gas loss through permeable magma. Journal of Volcanology and Geothermal Research 143, 53–68.

Mueller, S., Melnik, O., Spieler, O., Scheu, B., Dingwell, D.B., 2005. Permeability and degassing of dome lavas undergoing rapid decompression: an experimental determination. Bulletin of Volcanology 67, 526–538.

Nara, Y., Meredith, P.G., Yoneda, T., Kaneko, K., 2011. Influence of macro-

fractures and micro-fractures on permeability and elastic wave velocities in basalt at elevated pressure. Tectonophysics 503, 52–59.

Okumura, S., Nakamura, M., Uesugi, K., Nakano, T., Fujioka, T., 2013. Coupled effect of magma degassing and rheology on silicic volcanism. Earth and Planetary Science Letters 362, 163–170.

Papale, P., 1999. Strain-induced magma fragmentation in explosive eruptions. Nature 397, 425–428.

Piggott, A.R., Elsworth, D., 1992. Analytical models for flow through obstructed domains. Journal of Geophysical Research: Solid Earth 97, 2085–2093.

Plail, M., Edmonds, M., Humphreys, M.C., Barclay, J., Herd, R.A., 2014. Geochemical evidence for relict degassing pathways preserved in andesite. Earth and Planetary Science Letters 386, 21–33.

Renard, P., De Marsily, G., 1997. Calculating equivalent permeability: a review. Advances in water resources 20, 253–278.

Renard, P., Genty, A., Stauffer, F., 2001. Laboratory determination of full permeability tensor. Journal of Geophysical Research 106, 26–443.

Schauroth, J., Wadsworth, F.B., Kennedy, B., von Aulock, F.W., Lavallée, Y., Damby, D.E., Vasseur, J., Scheu, B., Dingwell, D.B., 2016. Conduit margin heating and deformation during the ad 1886 basaltic plinian eruption at tarawera volcano, new zealand. Bulletin of volcanology 78, 12.

Smith, J., Miyake, Y., Oikawa, T., 2001. Interpretation of porosity in dacite lava domes as ductile–brittle failure textures. Journal of Volcanology and Geothermal Research 112, 25–35.

Stinton, A.J., Cole, P.D., Stewart, R.C., Odbert, H.M., Smith, P., 2014. The 11 february 2010 partial dome collapse at soufrière hills volcano, montserrat. Geological Society, London, Memoirs 39, 133–152.

Tidwell, V.C., 1996. Laboratory investigation of constitutive property upscaling in volcanic tuffs. Technical Report. Sandia National Labs., Albuquerque, NM (United States).

Tuffen, H., Dingwell, D., 2005. Fault textures in volcanic conduits: evidence for seismic trigger mechanisms during silicic eruptions. Bulletin of Volcanology 67, 370–387.

Venezky, D., Rutherford, M., 1997. Preeruption conditions and timing of dacite-andesite magma mixing in the 2.2 ka eruption at mount rainier. Journal of Geophysical Research: Solid Earth 102, 20069–20086.

Vona, A., Romano, C., Dingwell, D., Giordano, D., 2011. The rheology of crystal-bearing basaltic magmas from stromboli and etna. Geochimica et Cosmochimica Acta 75, 3214–3236.

Wadsworth, F.B., Vasseur, J., Llewellin, E.W., Dobson, K.J., Colombier, M., von Aulock, F.W., Fife, J.L., Wiesmaier, S., Hess, K.U., Scheu, B., et al., 2017. Topological inversions in coalescing granular media control fluid-flow regimes. Physical Review E 96, 033113.

Wadsworth, F.B., Vasseur, J., Scheu, B., Kendrick, J.E., Lavallée, Y., Dingwell, D.B., 2016. Universal scaling of fluid permeability during volcanic welding and sediment diagenesis. Geology 44, 219–222.

Warren, J., Price, H., 1961. Flow in heterogeneous porous media. Society of Petroleum Engineers Journal 1, 153–169.

Watanabe, T., Shimizu, Y., Noguchi, S., Nakada, S., 2008. Permeability measurements on rock samples from unzen scientific drilling project drill hole 4 (usdp-4). Journal of Volcanology and Geothermal Research 175, 82–90.

Westrich, H.R., Eichelberger, J.C., 1994. Gas transport and bubble collapse in rhyolitic magma: an experimental approach. Bulletin of Volcanology 56, 447–458.